# Assessing Future Changes in the East Asian Summer Monsoon Using CMIP5 Coupled Models

KYONG-HWAN SEO, JUNG OK, AND JUN-HYEOK SON

*Department of Atmospheric Sciences, Division of Earth Environmental System, Pusan National University, Busan, South Korea*

DONG-HYUN CHA

*Department of Atmospheric Sciences, Division of Earth Environmental System, Ulsan National Institute of Science and Technology, Ulsan, South Korea*

(Manuscript received 18 September 2012, in final form 1 April 2013)

ABSTRACT

Future changes in the East Asian summer monsoon (EASM) are estimated from historical and Representative Concentration Pathway 6.0 (RCP6) experiments of the fifth phase of the Coupled Model Intercomparison Project (CMIP5). The historical runs show that, like the CMIP3 models, the CMIP5 models produce slightly smaller precipitation. A moisture budget analysis illustrates that this precipitation deficit is due to an underestimation in evaporation and ensuing moisture flux convergence. Of the two components of the moisture flux convergence (i.e., moisture convergence and horizontal moist advection), moisture convergence associated with mass convergence is underestimated to a greater degree.

Precipitation is anticipated to increase by 10%–15% toward the end of the twenty-first century over the major monsoonal front region. A statistically significant increase is predicted to occur mostly over the Baiu region and to the north and northeast of the Korean Peninsula. This increase is attributed to an increase in evaporation and moist flux convergence (with enhanced moisture convergence contributing the most) induced by the northwestward strengthening of the North Pacific subtropical high (NPSH), a characteristic feature of the future EASM that occurred in CMIP5 simulations. Along the northern and northwestern flank of the strengthened NPSH, intensified southerly or southwesterly winds lead to the increase in moist convergence, enhancing precipitation over these areas. However, future precipitation over the East China Sea is projected to decrease. In the EASM domain, a local mechanism prevails, with increased moisture and moisture convergence leading to a greater increase in moist static energy in the lower troposphere than in the upper troposphere, reducing tropospheric stability.

## 1. Introduction

The East Asian summer monsoon (EASM) is one of the most important large-scale circulation systems that impact the climate and weather in the East Asian region. Future projections of precipitation associated with the EASM in a warming climate have been examined in many previous studies using coupled models from the Intergovernmental Panel on Climate Change (IPCC)'s third phase of the Coupled Model Intercomparison Project (CMIP3) (e.g., Kitoh and Uchiyama 2006; Min et al. 2006; Zhou and Yu 2006; Kripalani et al. 2007; Lu et al. 2007; Chen and Sun 2009; Lu and Fu 2010; Kusunoki and Arakawa 2012; Seo and Ok 2013). The summer monsoonal rainfall over central and northern China, the Korean Peninsula, and Japan is expected to increase by 8%–20% near the end of the twenty-first century owing to global warming (Min et al. 2006; Kripalani et al. 2007; Kusunoki and Arakawa 2012; Seo and Ok 2013). This increase is mainly attributed to enhanced moist southerly flows over coastal East Asia (Lu et al. 2007).

Recently, several studies presented future projections of the East Asian monsoon using the CMIP5 models. For example, Lee and Wang (2013) demonstrated that the significant increase in summer precipitation over the entire Asian monsoon region is mainly attributable to

*Corresponding author address:* Dr. Kyong-Hwan Seo, Department of Atmospheric Sciences, Pusan National University, Busan 609735, South Korea.
E-mail: khseo@pusan.ac.kr

DOI: 10.1175/JCLI-D-12-00694.1

the enhancement and westward extension of the North Pacific subtropical high and significant increase of atmospheric moisture over the region, and Hsu et al. (2012) showed that most models in the CMIP3 and CMIP5 project an increase of global monsoon area and precipitation under global warming mainly attributable to the increases of moisture convergence and surface evaporation. These studies examined the global monsoon approach, but here we present future projections of the EASM in more detail. The models used in their work and the current study are not the same, so different results may appear. For example, Lee and Wang (2013) suggested a westward shift of the Pacific subtropical high, whereas our result shows a northwestward shift, so an increase in precipitation is prominent to the north of the Korean Peninsula (~38°–48°N, 120°–140°E). Moreover, both studies used the representative concentration pathway 4.5 (RCP4.5) simulations that have radiative forcing equilibrium about 4.5 $W m^{-2}$, while we analyze the simulations from the future climate scenario based on representative concentration pathway 6.0 (RCP6) because its $CO_2$ concentration is most similar to the Special Report on Emissions Scenarios (SRES) A1B, which was the mostly used scenario for the analysis of future climate in many previous studies. More detailed information about the scenario can be found in section 2.

The objectives of the present study are 1) to compare the performance of CMIP5 models with CMIP3 models associated with the EASM, which is done using a skill score estimated from correlation and normalized standard deviation, 2) to investigate future projections of the EASM with enhanced credibility using good models selected among 23 CMIP5 models, under the RCP6 scenario, and 3) to examine the major physical factors in future changes in the EASM.

## 2. Datasets and methods

In this study, two main observational datasets are used: the Climate Prediction Center (CPC) Merged Analysis of Precipitation (CMAP) (Xie and Arkin 1997) and the National Centers for Environmental Prediction–Department of Energy (NCEP–DOE) Reanalysis-2 (Kanamitsu et al. 2002). For the model data, we use the World Climate Research Programme's CMIP5 multimodel datasets.

The historical run (consistent with observations) was made with changing conditions in atmospheric composition because of anthropogenic and volcanic influences, solar forcing, emissions or concentrations of short-lived species and natural and anthropogenic aerosols or their precursors, and land use (Taylor et al. 2012). For ease of comparison, the datasets are interpolated into a 2.5° × 2.5° longitude–latitude grid for the 21-yr periods from 1979 to 1999.

For future climate projection, we used the RCP6 simulation because its $CO_2$ concentration is most similar to the SRES A1B under the IPCC Fourth Annual Report. RCP6 assumes that the target radiative forcing will increase and then stabilize at about 6.0 $W m^{-2}$ after 2100. For all experiments (historical run and RCP6 run), the first ensemble member (r1i1p1) was used in our analysis. The RCP6 simulations for the 21-yr periods from 2079 to 2099 are used. All data analyzed are monthly data.

The major East Asian monsoon region is defined as 25°–50°N and 100°E–180°. All analyses are conducted for the boreal summer season [June–August (JJA)]. To examine the overall performance of CMIP5 models compared to CMIP3 models and exclude the poorly performing models in simulating precipitation fields, the Taylor (2001) analysis is performed for climatological summer mean and interannual standard deviation distributions.

A measure of skill score $S$ for precipitation is calculated as

$$S = \frac{4(1+R)}{\left(\sigma + \frac{1}{\sigma}\right)^2 (1+R_0)}, \tag{1}$$

where $R$ is the pattern correlation between observation and simulation, $\sigma$ is simulated spatial standard deviation divided by that of observation (so it is normalized spatial standard deviation), and $R_0$ is an achievable maximum correlation (here set as 1). Therefore, $S$ evaluates both the pattern correlation and normalized spatial standard deviation simultaneously. Using these two sets of $S$ scores, the skills are averaged and models are ranked. The available CMIP5 outputs are 23 models (for CMIP3, they are 22 models). Utilizing previous values of correlation and normalized standard deviation used in discerning good and poor models in CMIP3 simulations (Seo and Ok 2013), a threshold of 0.77 is selected. Finally, the eight lowest-performing models are excluded for ensemble composite for the present-day climate. The selected 15 good models (having $S$ scores of 0.78–0.90) are CCSM4, CSIRO Mk3.6.0, GFDL-ESM2G, GFDL-ESM2M, GISS-E2-R, HadCM3, HadGEM2-CC, HadGEM2-ES, IPSL-CM5A-MR, MIROC-ESM-CHEM, MIROC4h, MIROC5, MPI-ESM-LR, MRI-CGCM3, and NorESM1-M. Of these 15 models, 8–15 models whose data for specific variables are currently available (Table 1) are used to determine the best future projections of the EASM.

TABLE 1. Description of the CMIP5 variables used in the study. Bold indicates good models selected among 23 CMIP5 models. PR is precipitation, HUS is specific humidity, Wind is *u* and *v* winds, GPH is geopotential height, and SAT is surface air temperature.

| | | PR | | HUS | | Wind | | GPH | | SAT | |
|---|---|---|---|---|---|---|---|---|---|---|---|
| PCMDI variables | Model name expansions | 20C | 21C | 20C | 21C | 20C | 21C | 20C | 21C | 20C | 21C |
| **CCSM4** | Community Climate System Model, version 4 | ● | ● | ● | ● | ● | ● | ● | ● | ● | ● |
| **CSIRO Mk3.6.0** | Commonwealth Scientific and Industrial Research Organisation Mark, version 3.6.0 | ● | ● | ● | ● | ● | ● | ● | | ● | ● |
| **GFDL-ESM2G** | Geophysical Fluid Dynamics Laboratory Earth System Model with Generalized Ocean Layer Dynamics (GOLD) component (ESM2G) | ● | ● | ● | ● | ● | ● | ● | ● | ● | ● |
| **GFDL-ESM2M** | Geophysical Fluid Dynamics Laboratory Earth System Model with Modular Ocean Model 4 (MOM4) component (ESM2M) | ● | ● | ● | ● | ● | ● | ● | ● | ● | ● |
| **GISS-E2-R** | Goddard Institute for Space Studies Model E, coupled with the Russell ocean model | ● | ● | ● | ● | ● | ● | ● | ● | ● | ● |
| **HadCM3** | Hadley Centre Coupled Model, version 3 | ● | | | | | | ● | | ● | |
| **HadGEM2-CC** | Hadley Centre Global Environment Model, version 2–Carbon Cycle | ● | | ● | | ● | | ● | | ● | |
| **HadGEM2-ES** | Hadley Centre Global Environment Model, version 2–Earth System | ● | ● | ● | ● | ● | ● | ● | | ● | ● |
| **IPSL-CM5A-MR** | L'Institut Pierre-Simon Laplace Coupled Model, version 5, coupled with NEMO, mid resolution | ● | | ● | | ● | | | | | ● |
| **MIROC-ESM-CHEM** | Model for Interdisciplinary Research on Climate, Earth System Model, Chemistry Coupled | ● | ● | ● | ● | ● | ● | ● | ● | ● | ● |
| **MIROC4h** | Model for Interdisciplinary Research on Climate, version 4 (high resolution) | ● | | | | | | ● | | ● | |
| **MIROC5** | Model for Interdisciplinary Research on Climate, version 5 | ● | ● | ● | ● | ● | ● | ● | ● | ● | ● |
| **MPI-ESM-LR** | Max Planck Institute Earth System Model, low resolution | ● | | ● | | ● | | ● | | ● | |
| **MRI-CGCM3** | Meteorological Research Institute Coupled Atmosphere–Ocean General Circulation Model, version 3 | ● | ● | ● | ● | ● | ● | ● | ● | ● | ● |
| **NorESM1-M** | Norwegian Earth System Model, version 1 (intermediate resolution) | ● | ● | ● | ● | ● | ● | ● | ● | ● | ● |
| CanCM4 | Fourth Generation Canadian Coupled Global Climate Model | ● | | | | | | ● | | | |
| CanESM2 | Second Generation Canadian Earth System Model | ● | | ● | | ● | | | | ● | |
| GISS-E2H | Goddard Institute for Space Studies Model E, coupled with the HYCOM ocean model | ● | | ● | | ● | | | | ● | |
| IPSL-CM5A-LR | L'Institut Pierre-Simon Laplace Coupled Model, version 5, coupled with NEMO, low resolution | ● | ● | ● | ● | ● | ● | ● | | ● | ● |
| BCC_CSM1.1 | Beijing Climate Center, Climate System Model, version 1.1 | ● | ● | ● | ● | ● | ● | ● | ● | ● | ● |
| GFDL CM3 | Geophysical Fluid Dynamics Laboratory Climate Model, version 3 | ● | ● | ● | | ● | | | | ● | ● |
| INM-CM4.0 | Institute of Numerical Mathematics Coupled Model, version 4.0 | ● | | ● | | ● | | ● | | ● | |
| MIROC-ESM | Model for Interdisciplinary Research on Climate, Earth System Model | ● | ● | ● | ● | ● | ● | ● | ● | ● | ● |

## 3. Results

### *a. Model performance in the present climate*

The proper projection of future precipitation change requires identification of poorly performing models prior to ensemble composite in order to avoid degradation of the ensemble forecast skill (Krishnamurti et al. 2000). To evaluate the overall skill in reproducing the present-day precipitation fields, the Taylor diagram analysis is applied to the CMIP5 models (Fig. 1). It is evident that both the climatological seasonal mean (Fig. 1a) and interannual standard deviation (Fig. 1b) fields for CMIP5 models are greatly improved over CMIP3 models in terms of both pattern correlation

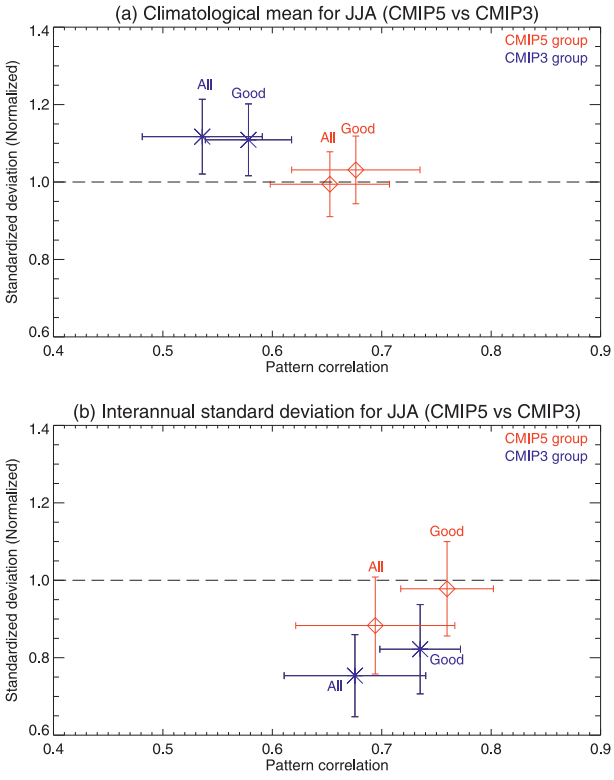


FIG. 1. Pattern correlation and spatial standardized deviation ratio between observation and CMIP5 (red) and CMIP3 (blue) all- and good-model ensembles for (a) the climatological seasonal mean and (b) interannual standard deviation fields. Horizontal and vertical lines denote intermodel standard deviations.

(abscissa in the figure) and spatial standardized deviation ratio (ordinate in the figure; unity means perfect model simulation). In particular, the all-model average pattern correlation of the climatological seasonal mean increases by more than 20% compared to the CMIP3 model, and spatial standardized deviation ratios for the CMIP5 models are close to unity. In addition, several highest and lowest skill score *S* models produce much better pattern resemblance to observation for the CMIP5 models compared to the CMIP3 models (not shown). Simulation skills calculated from excluding the eight models that perform the lowest skills among the analyzed models exhibit similar improvements. The composite using only these models is referred to as a good-model ensemble in this study. The good-model ensemble includes the intermediate-performing models as well as high-performing top models in order to increase the sample size for statistical testing of the warm climate projections. However, CMIP5 models also show a wide range of correlation values and standardized deviation ratios, similar to CMIP3 models.

### *b. Present-day model simulations*

Figure 2 shows the summer mean precipitation, 850-hPa moisture flux and its magnitude, 850-hPa geopotential height, and surface air temperature for the observations and good-model ensembles. In Fig. 2a, a peculiar rainband associated with the mei-yu–Changma–Baiu front is apparent, ranging from the east-central part of China through the Korean Peninsula to Japan. In the good-model ensemble (Fig. 2b), the Baiu front over Japan and its nearby oceans is well reproduced, but the model exhibits difficulty in simulating the local maximum associated with the mei-yu front over the lower reaches of the Yangtze River. In general, the good-model ensemble mean shows a weaker rainfall intensity over the major band, as is similarly shown in CMIP3 model simulations (e.g., Kusunoki and Arakawa 2012; Seo and Ok 2013; also in Fig. A1). This dry bias associated with the East Asian monsoonal front is a common problem in most contemporary climate models. It also produces unrealistically excessive precipitation over central inland China.

The second row of panels in Fig. 2 shows that the pattern of the 850-hPa moisture flux vector is effectively well simulated in the good-model ensemble with a slightly underestimated moisture flux intensity. The reasonable simulation of the moisture flux comes from the realistic representation of the North Pacific subtropical high (NPSH) (third row), one of the most important components of the EASM system. Other circulation fields are also examined. Sea level pressure and upper-level circulation (not shown) also demonstrate good correspondence with observations. The bottom panels of Fig. 2 show the composite surface air temperature field, which is also well reproduced by the model ensemble, with the East Asian continent being much warmer than the ocean, as in observations.

### *c. Future climate projections*

Future projection for the 21-yr period from 2079 to 2099 over East Asia using (8–15) available good-model simulations under the RCP6 scenario are presented in Fig. 3. The spatial pattern of precipitation in the future climate (top panel of 3a) is very similar to that of the present-day climate (top panel of Fig. 2b), showing a general increase over the whole region (top panel of Fig. 3b). The precipitation intensity strengthens by 10%–15% (Fig. 4a). The difference field between the future and present climate (top panel of Fig. 3b) exhibits a prominent increase in precipitation mainly over the Baiu frontal region (~30°–40°N, 135°–160°E) and the region north of the Korean Peninsula (~38°–48°N, 120°–140°E). The change in the latter region has not been

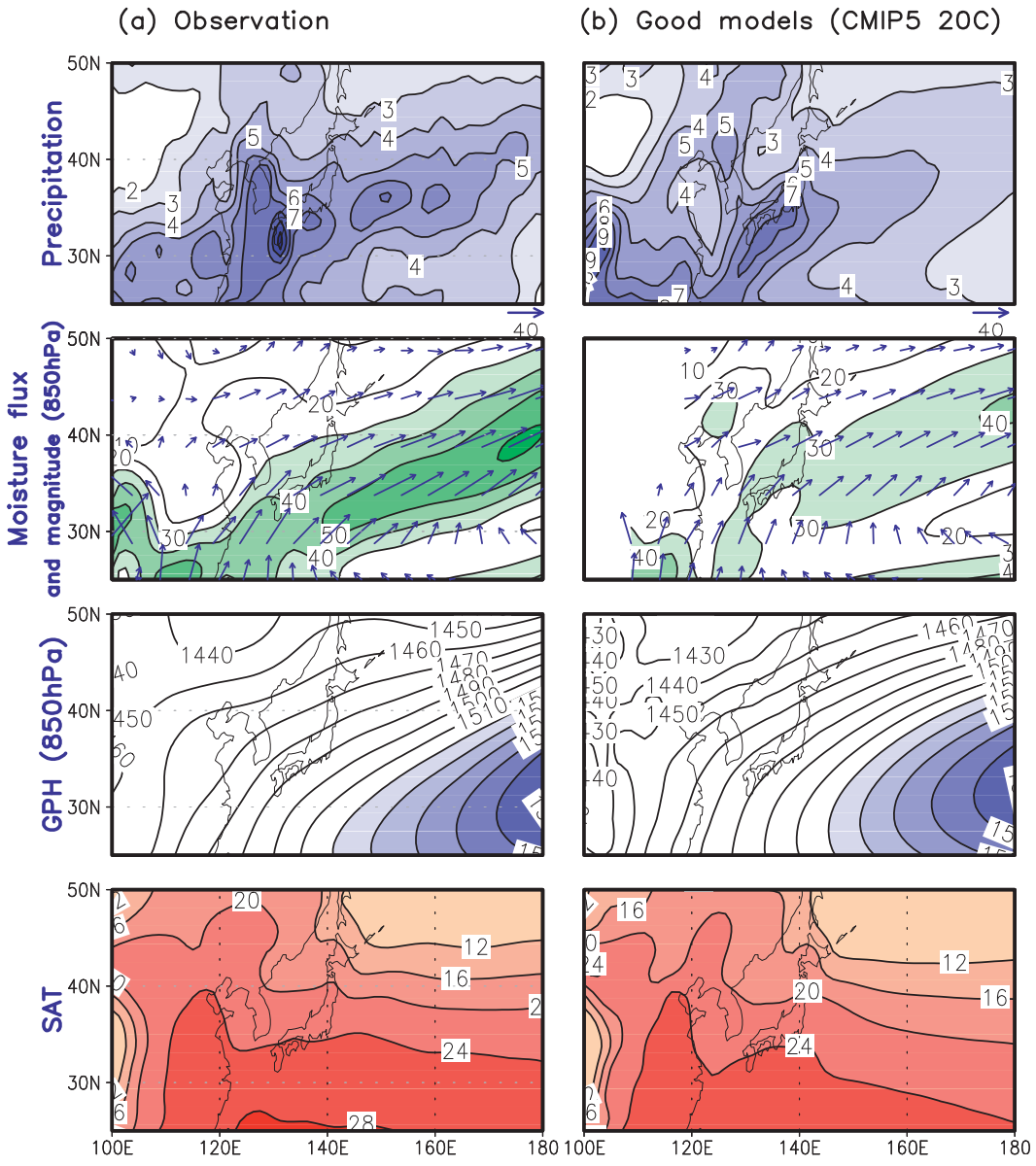


FIG. 2. Distribution of JJA mean precipitation (mm day$^{-1}$), moisture flux (vector) and its magnitude (shading) at 850 hPa (g kg$^{-1}$ m s$^{-1}$), 850-hPa geopotential height (m), and surface air temperature (°C) over the EASM region for (a) observations and (b) CMIP5 good-model ensemble mean for the present-day climate (1979–99).

previously identified. A plot of interannual variance of precipitation shows the formation of the local maximum over this area, even stronger than over the major rainband of the Baiu region (not shown), implying the greater degree of precipitation variability in this region. This is a relatively dry region, so the future monsoon change would contribute positively to the hydrological resources. On the other hand, a local maximum in the precipitation increase over southern inland China (near 30°N, 100°E; top panel of Fig. 3b and Fig. 4a) is not statistically significant, so we cannot be sure of future change in this region.

Precipitation increases seen in Figs. 3 and 4a are mainly attributed to increases in both evaporation and moisture flux over the EASM domain. About a 30%–50% increase in moisture flux is found over Japan and its eastern oceans and to the north of the Korean peninsula (Fig. 4b). Because of a warmer climate in the future (bottom panel of Fig. 3b), the lower-level specific humidity increases over the entire EASM region (Fig. 4c). Along the major EASM rainband, it increases by ~20%–30%. In addition, the northwestward expansion or intensification of the NPSH is evident in the future

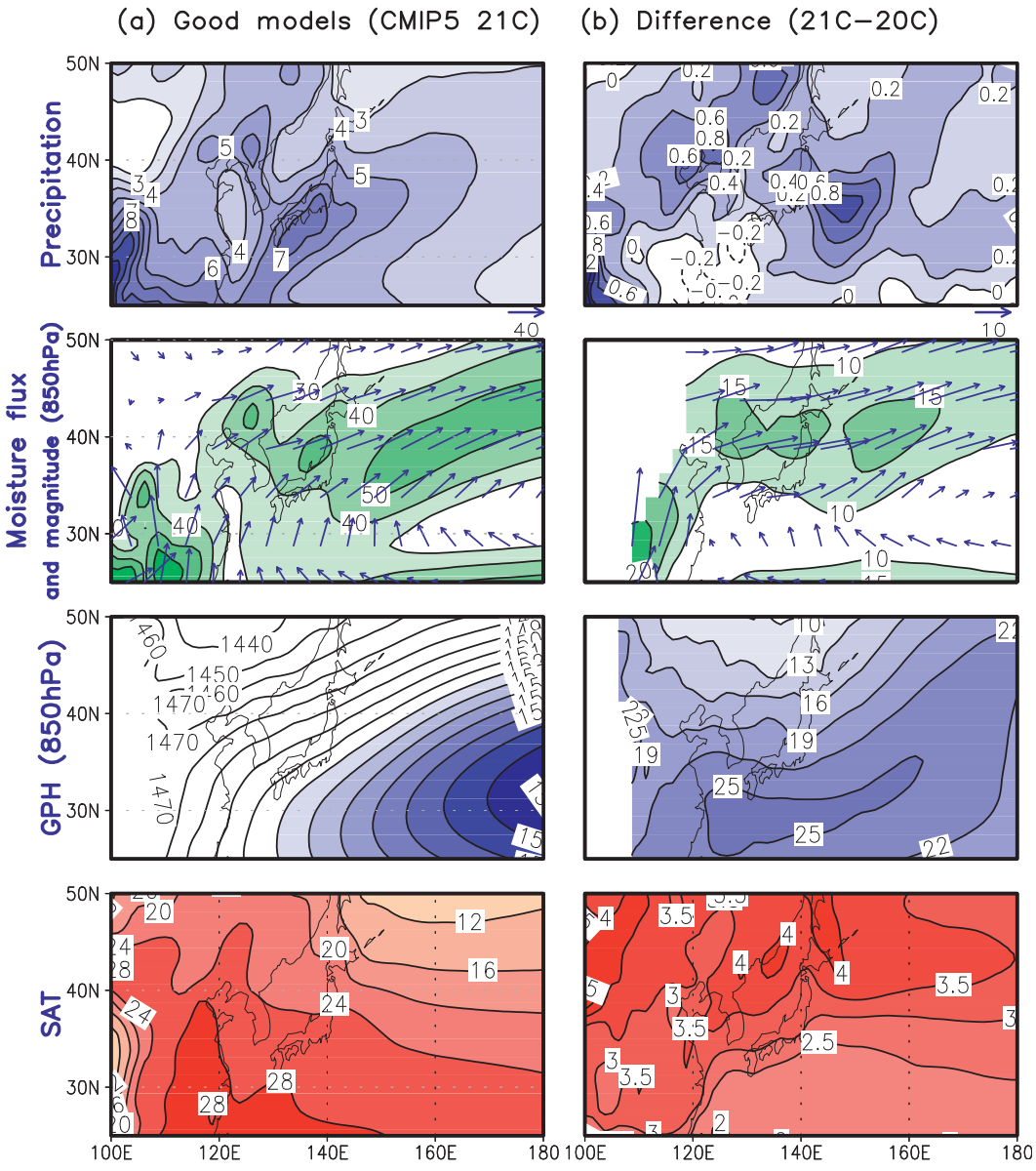


FIG. 3. As in Fig. 2, but for (a) the future climate scenario (21C: 2079–99) and (b) the difference between the 21C and 20C simulations.

climate scenario (third panel of Fig. 3) with the center of the low-level geopotential height anomaly located south or southeast of Japan (third panel of Fig. 3b). The westward strengthening of the NPSH in response to the observed Indian Ocean–western Pacific warming during the latter half of the twentieth century has been studied by Zhou et al. (2009). Recently, Seo et al. (2012) demonstrated that the northwestward intensification of the NPSH induced anomalously stronger southerly winds, leading to heavy rainfall for East Asian countries. Similarly, the stronger NPSH induces stronger southerly or southwesterly moisture flux (Fig. 3b), which is directed to the major EASM rainfall increase regions (i.e., over Japan and its nearby oceans and north of the Korean peninsula). Therefore, both enhanced water vapor and wind speed contributes to the increase in precipitation over the EASM region. The northwestward intensification of the NPSH in CMIP5 is a new feature and seems to be robust (since the similar spatial pattern found in RCP4.5 simulations (not shown) with an increase of the positive 850-hPa geopotential height is smaller by 15% compared to RCP6), and it is conjectured to be a result of an increase in convective forcing near the Philippine Sea in CMIP5 (not shown). By contrast, the

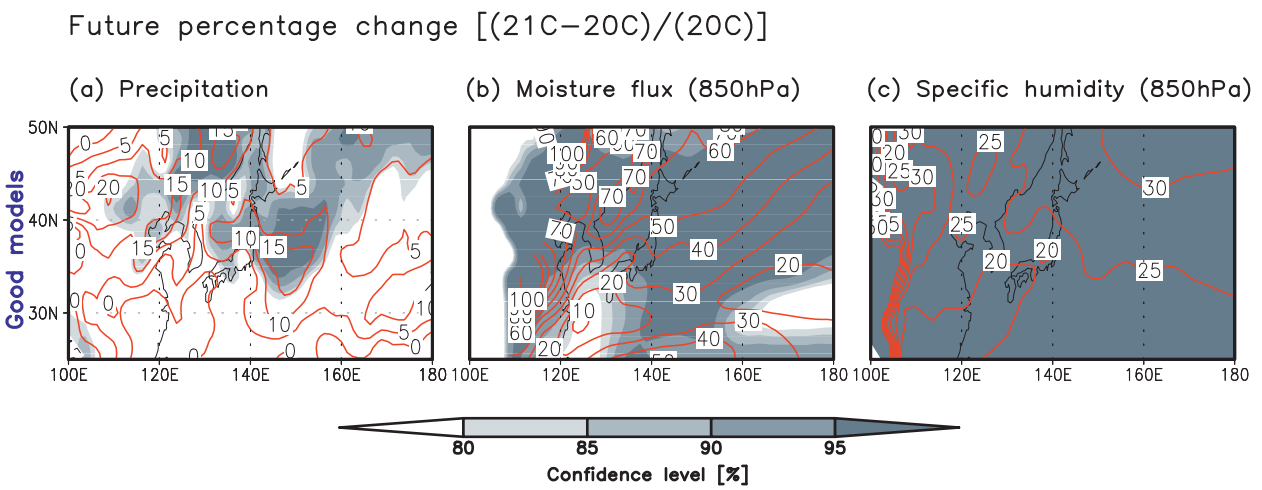


FIG. 4. Fractional percentage change (%, red contour) $[(21C - 20C)(20C)^{-1}]$ and statistical significance test (shading) for (a) precipitation, (b) moisture flux at 850 hPa, and (c) specific humidity at 850 hPa. Gray shading denotes the confidence level. Student's *t* test is used.

increase in convective forcing in the future in CMIP3 appears along the equator over the Pacific. The verification of this hypothesis will be performed in the future with a simplified general circulation model.

These CMIP5 results are compared with the CMIP3 good-model ensemble means (see the appendix). In CMIP3, the highly statistically significant increase in precipitation occurs over the major Baiu region (Seo and Ok 2013), whereas in CMIP5, along with the precipitation increase of the Baiu region, an additional region of precipitation increase emerges to the north of the Korean peninsula. The 850-hPa moisture flux strengthens over the more northern region than the one from CMIP3. This is related to the northwestward expansion or intensification of the NPSH in CMIP5 rather than an anticyclonic circulation anomaly centered over inland China (not the northwestern Pacific Ocean) in CMIP3. It is shown that the spatial patterns of precipitation and low-level moisture flux and geopotential height in the future climate are more consistent among these variables in CMIP5 than CMIP3. More detailed comparisons between CMIP5 and CMIP3 simulations can be found in the appendix.

To estimate important processes for this change in summertime precipitation, the moisture budget equation is analyzed (i.e., Yoon and Chen 2005; Hsu et al. 2012). The water vapor budget is calculated for the region of the major monsoonal rainband (26°–46°N, 114°–151°E):

$$\langle \nabla \cdot (q\mathbf{V}_H) \rangle = E - P + \text{Res}, \qquad (2)$$

where $q$ is specific humidity, $\mathbf{V}_H$ is horizontal wind, and $\langle\ \rangle$ represents a vertical integration from 1000 to 100 hPa. The variable $E$ is evaporation from the surface and $P$ is precipitation. The residual (Res) includes moisture tendency term (which is small), submonthly contributions, computational errors, biases in the data assimilation system, and inconsistency between the NCEP–DOE reanalysis and CMAP data. The first term in (2), moisture flux convergence, is further broken up into two terms: contributions from horizontal dry advection ($\mathbf{V}_H \cdot \nabla q$) and moisture divergence associated with mass divergence ($q\nabla \cdot \mathbf{V}_H$). Note that all data used are monthly data. Figure 5 shows the estimated value of each of these terms for the observation and good-model ensemble means. The moisture budget analysis shows that precipitation in the current climate is underestimated, as mentioned previously. This results from an underestimation in evaporation and ensuing moisture flux convergence. Of the two components of the moisture flux convergence, moisture convergence associated with mass convergence is more greatly underestimated (Fig. 5a).

The budget analysis also reveals that the domain-averaged precipitation increase is as much as ~7% because of the increases in both evaporation and moisture flux convergence (from Fig. 5b). The former results from the increased water vapor extent due to enhanced evaporation by increased surface temperature, and the latter comes from intensified southerly or southwesterly winds along the northwestern flank of the strengthened NPSH. The domain-averaged moisture advection is greater than that of moisture convergence. However, even if the domain-averaged evaporation is greatest among the three terms (Fig. 5b), the spatial pattern of evaporation (Fig. 6a) is significantly different from that of precipitation (Fig. 2b). Instead, moist convergence field (Fig. 6b) resembles precipitation field. Therefore,

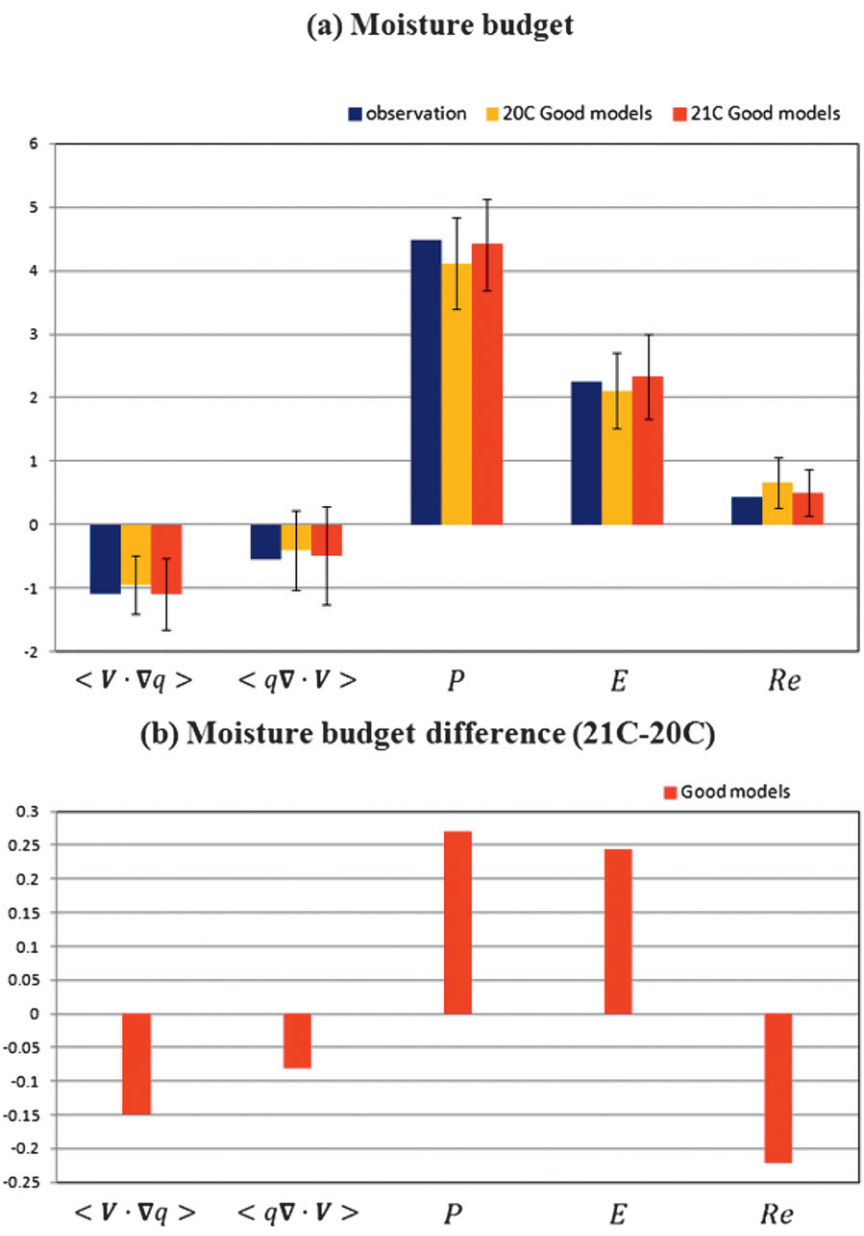


FIG. 5. Summer mean moisture budget of good-model ensemble for (a) observation, present-day climate (20C), and future climate (21C) and (b) future change (21C minus 20C) over the major rainband region. All units are mm day$^{-1}$. The error bar denotes the intermodel standard deviation.

the projected increase in precipitation over the Baiu region and to the north and northeast of the Korean Peninsula appears to be attributed to increases in water vapor content and moisture flux convergence (i.e., evaporation, moist advection, and moisture convergence), but enhanced moist convergence among these is the largest contributor to precipitation maxima to the north of the Korean Peninsula and to the east of Japan (Fig. 6b). An increase in precipitation over the sea between the Korean Peninsula and Japan is due to both the moist convergence and moisture advection terms. Another feature to note is that the future precipitation over the East China Sea (~32N°, 127°E) decreases, which is primarily due to strongly reduced moist convergence and moderately reduced moisture advection in this area (Fig. 6b). This reduced precipitation area leads to the domain-averaged moisture convergence being smaller than the domain-averaged moisture advection. On the

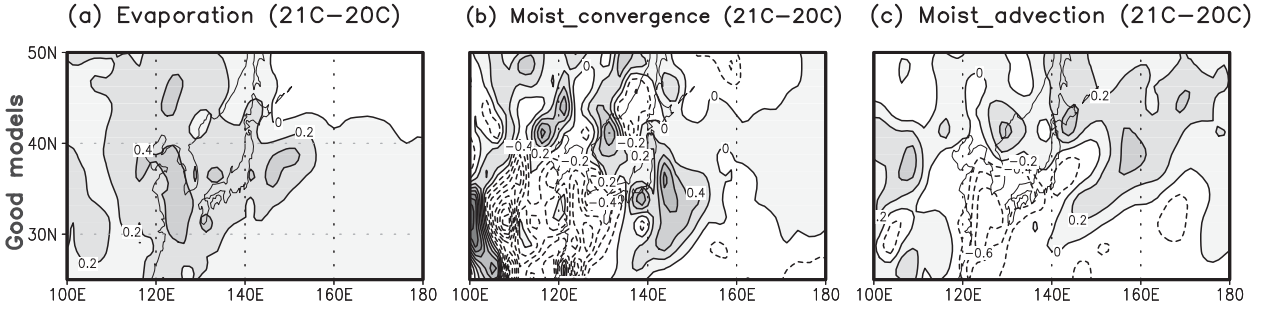


FIG. 6. Distributions of JJA mean differences in (a) evaporation, (b) moist convergence, and (c) moist advection between the 21C and 20C simulations (mm day$^{-1}$).

other hand, moisture advection (Fig. 6c) is responsible for an increase in precipitation to the north of the major increase region of precipitation over the eastern Sea of Japan (i.e., ~45N°, 165°E). Note that the relative importance between the moisture advection and convergence terms seems to be subject to large uncertainty, so a caution is needed. Nonetheless, the spatial distribution of moisture convergence is most similar to that of precipitation, so that major changes in local precipitation in the future may be determined by moisture convergence. To be more decisive, improved model fidelity in representing the EASM is of relevance.

A brief comparison with CMIP3 simulations is also done. Among the two components in the domain-averaged moisture flux convergence $[\nabla \cdot (q\mathbf{V}_H)]$, the future increase in moist convergence is greater in CMIP3 (see Seo and Ok 2013), whereas the moist advection increase is greater in CMIP5. Moreover, the future increase in moisture flux convergence is 50% greater than the increase in evaporation in CMIP3, but the increases in these two quantities are very similar in CMIP5. However, the major increases (decreases) in precipitation over the continental region to the north of the Korean Peninsula and the eastern Sea of Japan (over the East China Sea) are due mainly to an increase (decrease) in moisture convergence. The increase seen to the east of Japan is actually similar to the CMIP3 results, which also show an increase along the major Baiu frontal region resulting from the enhanced moist convergence.

To investigate whether the monsoon response to greenhouse gas forcing in the select models takes place via a local or remote process (Neelin and Held 1987; Seth et al. 2011; Giannini 2010), moist static energy (MSE) has been exploited over the EASM region. In the local mechanism, increased evaporation as a result of the surface response to anthropogenically enhanced radiative forcing leads to an increase in the MSE, a decrease in tropospheric stability, and an increase in precipitation (see Seth et al. 2011; Giannini 2010). The well-known ''rich get richer'' framework dominates in this case. Meanwhile, for the remote mechanism, large-scale tropospheric warming controls vertical stability. Therefore, we calculate the vertical stability using the MSE in the upper and lower troposphere. The MSE is defined as MSE = DSE + $Lq$, where the dry static energy (DSE) is defined as DSE = $c_pT + gZ$. Here, $L$ is the latent heat of evaporation, $q$ is specific humidity, $c_p$ is the specific heat at constant pressure, $T$ is the layer temperature, $g$ is gravity, and $Z$ is geopotential height. Since there is little water vapor in the upper troposphere, the MSE in the upper level is equivalent to DSE. So, as a measure of free tropospheric stability, the vertical gradient of MSE, which is defined as $\upsilon\text{MSE} = \text{DSE}_{200} - \text{MSE}_{850}$ (Held 2001; Seth et al. 2011), is calculated.

The change of $\upsilon$MSE between RCP6 and historical simulations is presented in Fig. 7a, where positive (negative) value denotes increased stability (instability). As seen in the figure, the $\upsilon$MSE decreases over the EASM domain, implying enhanced instability in the future and, thus, wetter EASM under global warming. To explore the cause of this increased instability, we decompose the $\upsilon$MSE terms into 200-hPa DSE and 850-hPa MSE. First, the upper-level DSE (Fig. 7b) shows an increased stability, which is mainly controlled by the temperature term $c_pT$ (Fig. 7c) [wherein geopotential height ($gZ$) change is negligible]. However, the greater positive change existent in the lower-level $\text{MSE}_{850}$ suggests a strongly enhanced instability across the domain (Fig. 7d). This is contributed mostly by the moisture term $Lq$, not by the DSE (Figs. 7e,f). The increase in the MSE due to the enhanced lower-level specific humidity is greater than that by the lower-level temperature change (Fig. 7g). Thus, the increased free tropospheric instability during the boreal summer is attributed to the greater increase in $\text{MSE}_{850}$ than in $\text{DSE}_{200}$. This change in the vertical gradient of the MSE is consistent with the local mechanism (Seth et al. 2011; Giannini 2010). These results demonstrate that an enhancement in precipitation in response to greenhouse gas forcing is due to a local process and increased evaporation plays a major role.

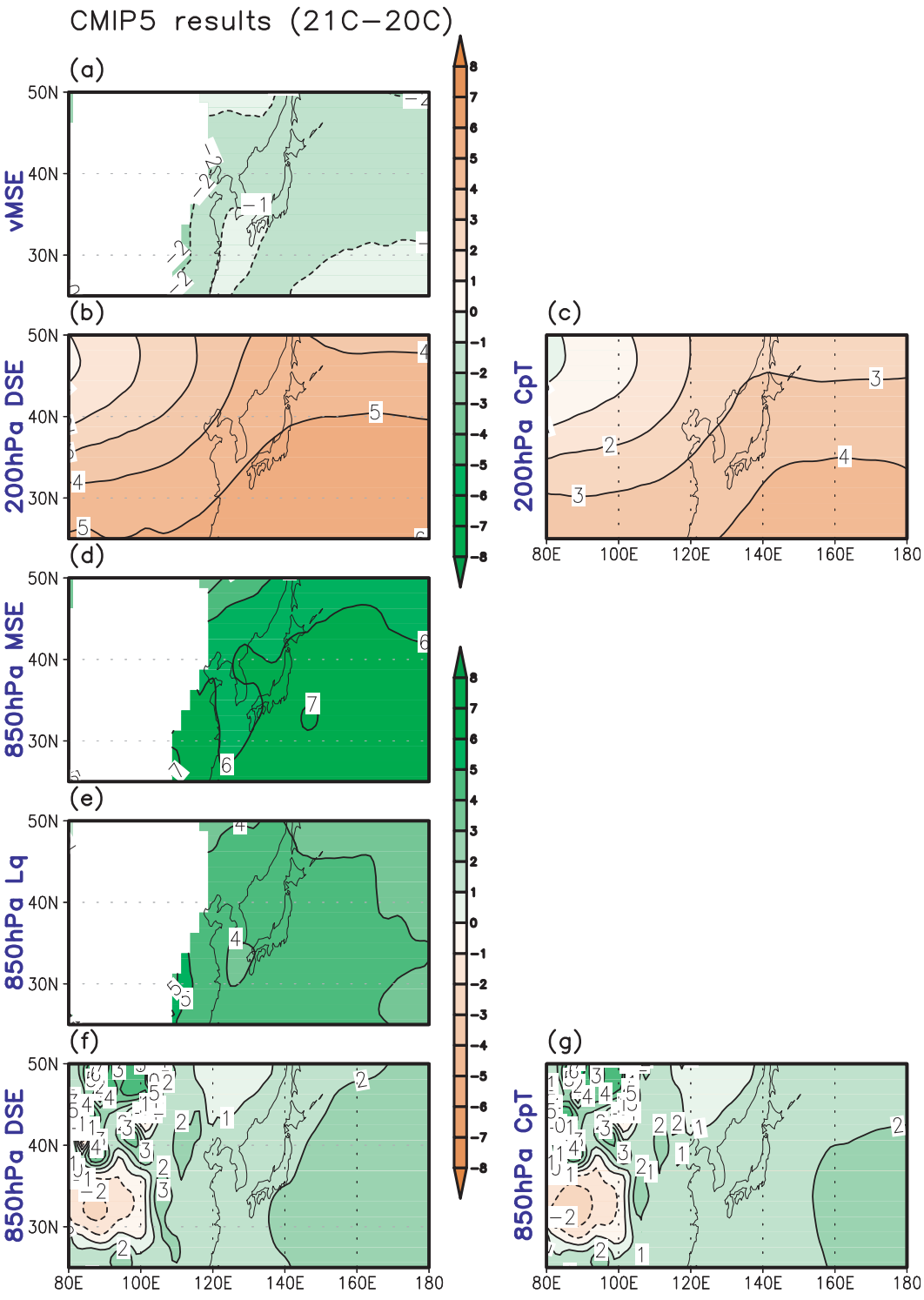


FIG. 7. Distributions of differences (21C minus 20C) in (a) vertical gradient of moist static energy (200–850 hPa MSE; kJ kg$^{-1}$); 200-hPa (b) DSE and (c) $c_p T$, where the positive difference indicates an increased stability (brown); and 850-hPa (d) MSE, (e) $Lq$, (f) DSE, and (g) $c_p T$, where positive differences indicate a decreased stability (green).

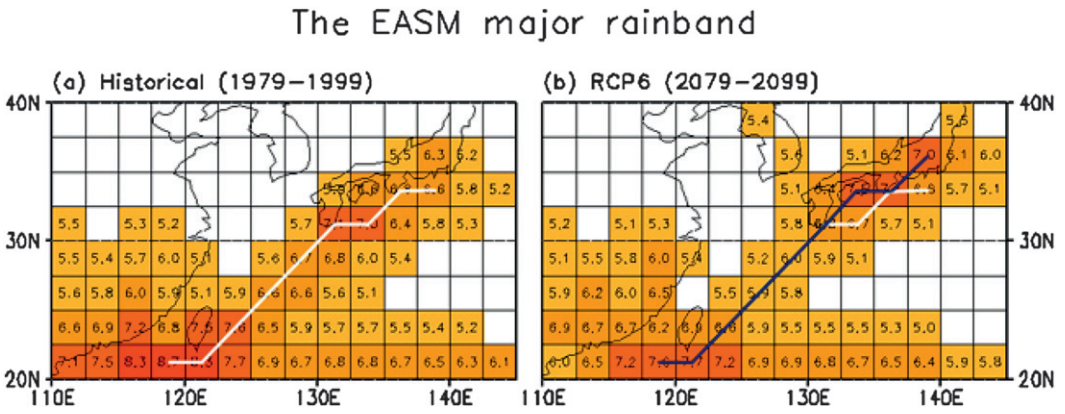


FIG. 8. JJA mean precipitation (mm day$^{-1}$) at each grid point for (a) the present-day climate and (b) future climate. The white line denotes an estimated monsoonal rainband in the good-model composite for present climate conditions; the blue line represents that for the future climate.

Finally, meridional movement of the monsoonal band in response to increased $CO_2$ forcing has been examined. Some previous studies have demonstrated an apparent southward shift of the EASM-related precipitation or precipitation anomalies (e.g., Yun et al. 2008; Li et al. 2010). Using CMIP5 good-model data, we examine the possible spatial shift of the monsoon front. This is done by connecting the local maximum precipitation intensities as shown in Fig. 8. It indicates little movement of the monsoonal major rainband, as has been similarly shown in previous CMIP3 analyses (Seo and Ok 2013).

## 4. Summary

Future changes in the amount and position of EASM precipitation have been estimated from CMIP5 climate model simulations under the RCP6 scenario. The prior comparison with CMIP3 historical simulations shows that CMIP5 models are, in general, found to better simulate the observed spatial and temporal precipitation patterns related to the EASM, compared to CMIP3 simulations.

For the proper composite of model simulations, the best-performing models from the historical run are selected through the first two moment statistics (i.e., mean and variance) of precipitation. The selected model ensemble mean in the present-day climate reasonably simulates the monsoonal rainband over East Asia during the summer season. However, as in CMIP3, the model composite produces slightly less precipitation, with the Baiu front aligned more steeply in the meridional direction than is shown in observations. A moisture budget analysis shows that this precipitation deficit is due to an underestimation in evaporation and ensuing moisture flux convergence. Of the two components of the moisture flux convergence, moisture convergence associated with mass convergence is more greatly underestimated. Even if the good models were selected solely from the precipitation statistics, the composite exhibited very realistic temperature and circulation fields, indicating the effectiveness of the applied selection criteria.

A moisture budget analysis demonstrates that the EASM domain-averaged precipitation increases by ~7% for the period of 2079–99 in the case of the RCP6 scenario because of increases in both evaporation [by the increased surface temperature of 2.0°–3.5°C (inferred from Fig. 3b)] and moisture flux convergence. However, precipitation over the major monsoon front-related region is anticipated to increase by as much as 10%–15%. A peculiar feature in the future EASM is a northwestward strengthening of the NPSH. Therefore, along the northern and northwestern flank of the strengthened NPSH, intensified southerly or southwesterly winds lead to an increase in moisture convergence, enhancing precipitation particularly over the Baiu region to the east of Japan and the continental region to the north of the Korean Peninsula. However, future precipitation over the East China Sea (~32N°, 127°E) decreases because of strongly reduced moist convergence and moderately reduced moisture advection in this area.

It is revealed that the increased moist content in the lower level as a result of response to anthropogenically enhanced radiative forcing leads to an increase in the MSE, decreasing tropospheric stability. This result implies that a local process as opposed to a remote mechanism operates for the EASM. Little meridional shift of the monsoonal major rainband is expected to occur in the future.

Although the CMIP5 models are greatly improved over CMIP3 models in terms of climatologically seasonal mean and interannual variability, we cannot guarantee

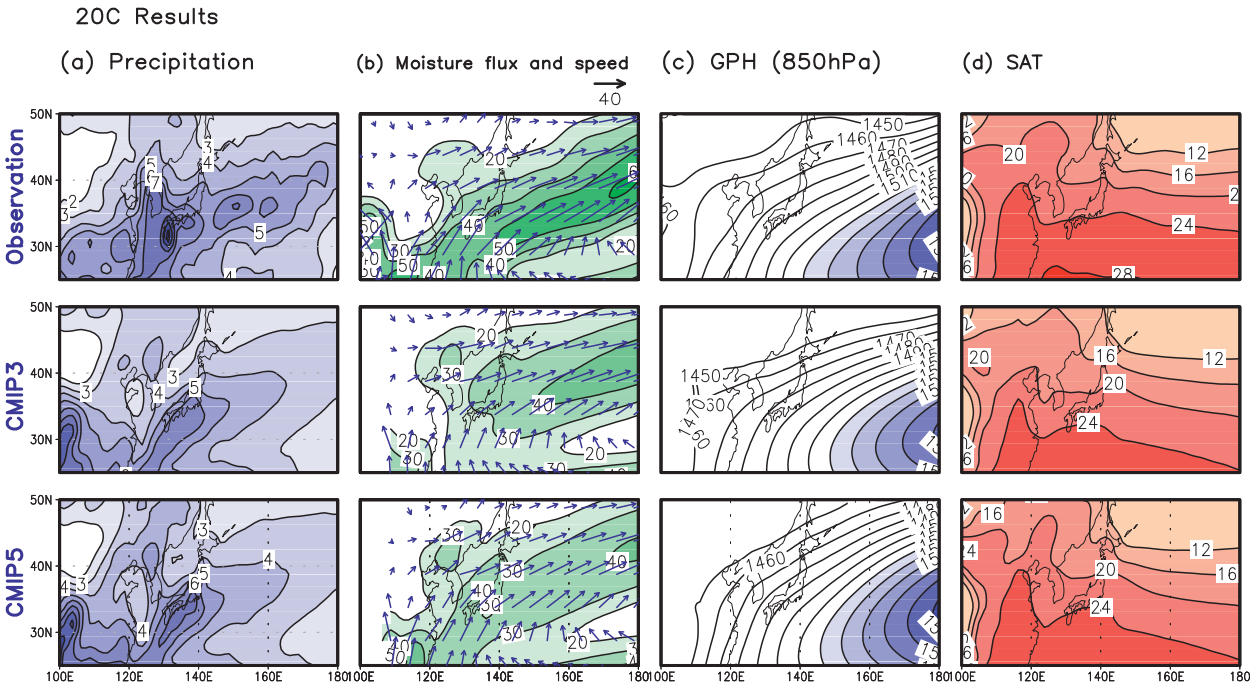


FIG. A1. Distributions of JJA mean (a) precipitation (mm day$^{-1}$), (b) moisture flux (vector) and its magnitude (shading) at 850 hPa (g kg$^{-1}$ m s$^{-1}$), (c) 850-hPa geopotential height (m), and (d) surface air temperature (°C) over the EASM region for (top) observations, (middle) CMIP3 good-model ensemble mean, and (bottom) CMIP5 good-model ensemble mean for the present-day climate (1979–99).

that the CMIP5 models more accurately predict the future climate change. Also, the residual term is not small enough to be ignored. Therefore, the results in this study are of limited importance. However, the spatial patterns of precipitation and low-level moisture flux and geopotential height in the future climate are more consistent each other in CMIP5 than CMIP3, so CMIP5 projections seem to be more reliable.

*Acknowledgments.* This work was funded by the Korea Meteorological Administration Research and Development Program under Grant CATER 2012-3071. This work was also supported by the National Research Foundation of Korea (NRF) Grant funded by the Korea government (MEST) (No. 2011-0015486). The authors would like to acknowledge the support from the Korea Institute of Science and Technology Information (KISTI). We acknowledge the World Climate Research Programme's Working Group on Coupled Modeling, which is responsible for CMIP, and we thank the climate modeling groups for producing and making available their model output. For CMIP the U.S. Department of Energy's Program for Climate Model Diagnosis and Intercomparison provides coordinating support and led development of software infrastructure in partnership with the Global Organization for Earth System Science Portals.

## APPENDIX

### The EASM in CMIP5 and CMIP3

CMIP5 models are greatly improved over CMIP3 models in the climatologically seasonal mean and interannual variability. For a more detailed comparison, we present CMIP3 and CMIP5 results side by side in Fig. A1. Good models in CMIP3 are selected based on the skill score ($S$), as in CMIP5 models in this paper. The select good models are 15 and 14 for CMIP5 and CMIP3, respectively. The used data list is shown in Table 1. It is seen in Fig. A1a that the observed pattern and intensity of precipitation are well simulated by the CMIP5 models, especially in southern Japan, whereas the CMIP3 models tend to underestimate the intensity of precipitation. Figure A1b shows the patterns of 850-hPa moisture flux vector and its magnitude. It is seen that southwesterly monsoonal moist flow over the East China Sea is better simulated in the CMIP5 models, which is due to a proper simulation of the lower-level geopotential height gradient, as shown in Fig. A1c. In the surface air temperature pattern (Fig. A1d), CMIP5 shows a better representation compared to CMIP3; CMIP3 produces a stronger underestimation over land area. Therefore, overall, the CMIP5 good models are in much better correspondence with observation

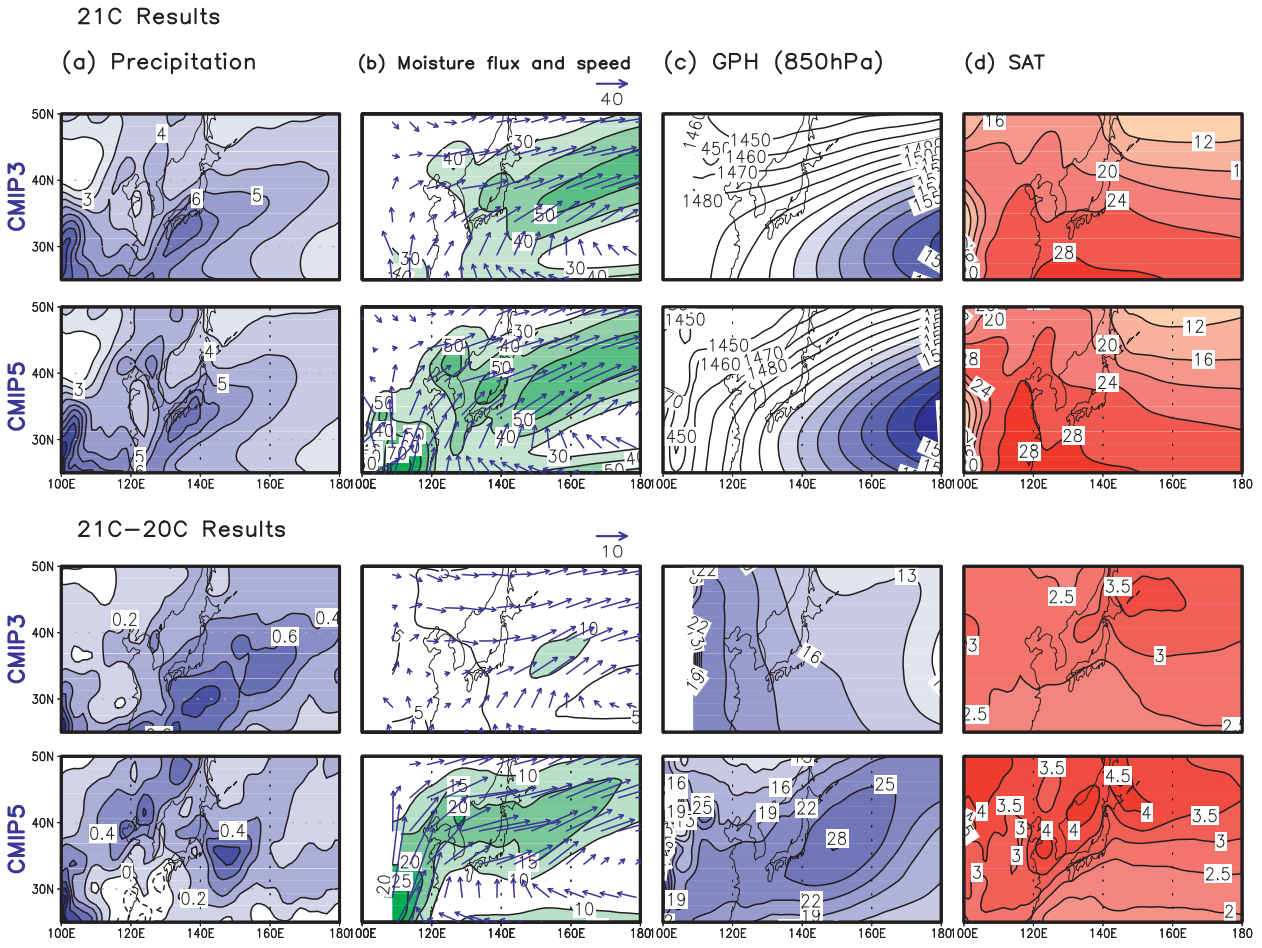


FIG. A2. As in Fig. A1, but for the future climate scenario (21C: 2079–99) and the difference between the 21C and 20C simulations.

than the CMIP3 good models in representing the present-day climate.

For future changes, we used the SRES A1B simulations for CMIP3 models and the RCP6 scenario for CMIP5 models. Note that these scenarios have differences in $CO_2$ forcing; A1B and RCP6 have $CO_2$ concentrations of 720 and 670 ppm, respectively, in the year 2100, indicating that the slightly smaller radiative forcing of the RCP6 scenario compared to the A1B scenario in this year. In Fig. A2, the upper panels denote the twenty-first-century (21C) results and the lower panels represent the future change [21C minus twentieth century (20C)] for the CMIP3 and CMIP5 models. The general patterns of precipitation for the CMIP5 models are similar to those of the CMIP3 models (upper panels of Fig. A2a). However, in the CMIP5 models, enhanced rainfall in the future occurs to the north and northeast of the Korean Peninsula and to the east of Japan (the bottom panel of Fig. A2a), whereas the CMIP3 models are projected to increase from the western Pacific toward the central Pacific (the third panel of Fig. A2a). In addition, the CMIP5 models show much larger increases in the strength of 850-hPa moisture flux than the CMIP3 models, especially over eastern China and the East China Sea, the Korean Peninsula, and central Japan (Fig. A2b). These differences between the CMIP3 and CMIP5 model ensemble means are presumably associated with changes in the lower-level geopotential height (Fig. A2c). That is, the northwestward strengthening of the NPSH is evident in CMIP5, so anticyclonic flow appears along the rim of this high anomaly, whereas a high anomaly center is over the Asian continent (not over the western north Pacific) with a weaker pressure gradient (Fig. A2c), which is odd. In light of this, the CMIP5 future projection is more reliable. Surface air temperatures from both the CMIP5 and CMIP3 models are projected to increase in the future (Fig. A2d). However, it is interesting to see that the temperature change in CMIP5 is greater than that of CMIP3 by ~0.5 K over most of the EASM domain, even if the radiative forcing of the former is smaller than that of the latter.

## REFERENCES


Chen, H. P., and J. Q. Sun, 2009: How the ''best'' models project the future precipitation change in China. *Adv. Atmos. Sci.,* **26,** 773–782, doi:10.1007/s00376-009-8211-7.

Giannini, A., 2010: Mechanisms of climate change in the semiarid African Sahel: The local view. *J. Climate,* **23,** 743–756.

Held, I. M., 2001: The partitioning of the poleward energy transport between the tropical ocean and atmosphere. *J. Atmos. Sci.,* **58,** 943–948.

Hsu, P.-C., T. Li, J.-J. Luo, H. Murakami, and A. Kitoh, 2012: Increase of global monsoon area and precipitation under global warming: A robust signal? *Geophys. Res. Lett.,* **39,** L06701, doi:10.1029/2012GL051037.

Kanamitsu, M., and Coauthors, 2002: NCEP–DOE AMIP-II Reanalysis (R-2). *Bull. Amer. Meteor. Soc.,* **83,** 1631–1643.

Kitoh, A., and T. Uchiyama, 2006: Changes in onset and withdrawal of the East Asian summer rainy season by multi-model global warming experiments. *J. Meteor. Soc. Japan,* **84,** 247–258.

Kripalani, R. H., J.-H. Oh, and H. S. Chaudhari, 2007: Response of the East Asian summer monsoon to doubled atmospheric $CO_2$: Coupled climate model simulations and projections under IPCC AR4. *Theor. Appl. Climatol.,* **87,** 1–28.

Krishnamurti, T. N., C. M. Kishtawal, Z. Zhang, T. Larow, D. Bachiochi, and E. Willford, 2000: Multimodel ensemble forecasts for weather and seasonal climate. *J. Climate,* **13,** 4196–4216.

Kusunoki, S., and O. Arakawa, 2012: Change in the precipitation intensity of the East Asian summer monsoon projected by CMIP3 models. *Climate Dyn.,* **38,** 2055–2072, doi:10.1007/s00382-011-1234-7.

Lee, J.-Y., and B. Wang, 2013: Future change of global monsoon in the CMIP5. *Climate Dyn.,* doi:10.1007/s00382-012-1564-0, in press.

Li, J. P., Z. W. Wu, Z. H. Jiang, and J. H. He, 2010: Can global warming strengthen the East Asian summer monsoon? *J. Climate,* **23,** 6696–6705.

Lu, R., and Y. Fu, 2010: Intensification of East Asian summer rainfall interannual variability in the twenty-first century simulated by 12 CMIP3 coupled models. *J. Climate,* **23,** 3316–3331.

——, Y. Li, and B. Dong, 2007: East Asian precipitation increase under the global warming. *J. Korean Meteor. Soc.,* **43,** 267–272.

Min, S.-K., S. Legutke, A. Hense, U. Cubasch, W.-T. Kwon, J.-H. Oh, and U. Schlese, 2006: East Asian climate change in the 21st century as simulated by the coupled climate model ECHO-G under IPCC SRES scenarios. *J. Meteor. Soc. Japan,* **84,** 1–26.

Neelin, J. D., and I. M. Held, 1987: Modeling tropical convergence based on the moist static energy budget. *Mon. Wea. Rev.,* **115,** 3–12.

Seo, K.-H., and J. Ok, 2013: Assessing future changes in the East Asian summer monsoon using CMIP3 models: Results from the best model ensemble. *J. Climate,* **26,** 1807–1817.

——, J.-H. Son, S.-E. Lee, T. Tomita, and H.-S. Park, 2012: Mechanisms of an extraordinary East Asian summer monsoon event in July 2011. *Geophys. Res. Lett.,* **39,** L05704, doi:10.1029/2011GL050378.

Seth, A., S. A. Rauscher, M. Rojas, A. Giannini, and S. J. Camargo, 2011: Enhanced spring convective barrier for monsoons in a warmer world? *Climatic Change,* **104,** 403–414.

Taylor, K. E., 2001: Summarizing multiple aspects of model performance in a single diagram. *J. Geophys. Res.,* **106,** 7183–7192.

——, R. J. Stouffer, and G. A. Meehl, 2012: An overview of CMIP5 and the experiment design. *Bull. Amer. Meteor. Soc.,* **93,** 485–498.

Xie, P., and P. A. Arkin, 1997: Global precipitation: A 17-year monthly analysis based on gauge observations, satellite estimates and numerical model outputs. *Bull. Amer. Meteor. Soc.,* **78,** 2539–2558.

Yoon, J.-H., and T.-C. Chen, 2005: Water vapor budget of the Indian monsoon depression. *Tellus,* **57A,** 770–782, doi:10.1111/j.1600-0870.2005.00145.x.

Yun, K.-S., S.-H. Shin, K.-J. Ha, A. Kitoh, and S. Kusunoki, 2008: East Asian precipitation change in the global warming climate simulated by a 20-km mesh AGCM. *Asia-Pac. J. Atmos. Sci.,* **44,** 233–247.

Zhou, T. J., and R. C. Yu, 2006: Twentieth century surface air temperature over China and the globe simulated by coupled climate models. *J. Climate,* **19,** 5843–5858.

——, and Coauthors, 2009: Why the western Pacific subtropical high has extended westward since the late 1970s. *J. Climate,* **22,** 2199–2215.